Fatigue Crack Propagation in Microlayer Composites of Polycarbonate and Poly(styrene–Acrylonitrile)

M. MA,* J. IM,[†] A. HILTNER, and E. BAER, *Center for Applied Polymer Research and Department of Macromolecular Science, Case Western Reserve University, Cleveland, Ohio 44106 and [†]The Dow Chemical Company, Midland, Michigan 48640*

Synopsis

The effect of layer thickness on fatigue crack propagation (FCP) in microlayer composites of polycarbonate (PC) and styrene–acrylonitrile copolymer (SAN) has been studied. Variation in layer thickness was achieved by increasing the number of layers from 49 to 776 while keeping the overall sheet thickness and composition the same. It was found that the 776 layer composite had a larger number of fatigue cycles from crack initiation to fracture, a longer stable crack length and higher value of critical strain energy release rate J_{1C}. Microscopic characterization of the damage zone and resulting fracture surface revealed a transition from SAN crazing to shear deformation as layer thickness decreased from 18 to 1 μm; the resulting plastic deformation and ductile fracture of the 776 layer composite was responsible for the enhanced FCP resistance. The ductile fracture mechanism produced a measurable temperature rise at the crack tip that revealed the stop-start nature of crack propagation.

INTRODUCTION

In previous studies, effects of composition and layer thickness on the deformation of microlayer composites with alternating layers of polycarbonate (PC) and styrene–acrylonitrile copolymer (SAN) were investigated.[1–3] In these studies, competition between SAN crazing or cracking and PC shearing mechanisms was related to the stress–strain behavior. By increasing the number of layers while keeping the overall sheet thickness and composition the same, a transition from brittle to ductile behavior was observed with decreasing layer thickness. Enhanced ductility of the composites with thinner SAN layers was attributed to the local stress state at the interface, which caused the SAN layers to deform in a shear mode.

It was subsequently demonstrated that the transition from crazing to shear deformation in SAN layers was responsible for differences in the damage zone at a stress concentrator such as a notch.[4] Characteristic microdeformation behavior of the layered structures produced a damage zone in a 49 layer composite composed of profuse crazing through the sheet thickness compared to the smaller zone in a 776 layer composite of the same composition, which showed distinctive skin-core features with shear yielding.

* Present address: Rogers Corporation, One Technology Dr., Rogers, CT 06263.

CCC 0021-8995/90/5-60669-16$04.00

It is well known that the damage zone ahead of a crack serves as an energy absorbing mechanism that can enhance resistance to fatigue crack propagation.[5-11] The present study was undertaken to determine how changes in the damage zone due to layer thickness affect fatigue crack propagation in the 49 and 776 layer composites.

EXPERIMENTAL

Materials

Microlayer composites comprised of alternating PC and SAN were supplied by The Dow Chemical Co. in the form of coextruded sheets; the outermost layer was always PC. The PC and SAN used were Merlon (Trademark, Mobay Chemical Co.) M-40 and Tyril (Trademark, The Dow Chemical Co.) 867-B, respectively. Composites with 49 and 776 layers were studied; both were 1.20 mm thick with a PC/SAN volume ratio of about 65/35. This resulted in individual layer thicknesses of PC and SAN in the 49 layer composite of 30 and 18 μm, respectively, and 2 and 1 μm, respectively, in the 776 layer composite.

Fatigue Testing

Rectangular fatigue specimens 20 mm wide with a single edge notch (SEN) were machined parallel to the extrusion direction. The 60° V-shaped notch had a 2.54 μm tip radius and a depth of 1 mm. The gauge length was about 60 mm when the specimen was mounted in the Instron testing machine for fatigue testing.

The loads for fatigue testing were within the nominally linear region of the stress–displacement curve which was identical for the two composites. The maximum and minimum loads of 14.6 and 2.9 MPa corresponded to 21 and 4% of the unnotched yield stress of the two composites (70 MPa). The frequency was approximately 0.2 Hz and the stress wave was a ramp mode. A video camera was used to record the crack length continuously during fatiguing for the purpose of determining the crack speed. At least 15 specimens of each composite were tested.

Microscopy

A traveling optical microscope with a camera was used to observe the damage zone during crack initiation and propagation. Resulting fracture surfaces were examined with both the transmission optical microscope (Olympus BH2) and scanning electron microscope (JEOL JEM-35CF). To examine the interior of the damage zone, a specimen was fatigued under the conditions previously described until the desired crack length was obtained; then the specimen was unloaded and subsequently roughly cut with a band saw to the approximate position desired within the damage zone, ground on a polishing wheel with fine sand paper to achieve the exact location, and finally polished with 1 μm aluminum oxide powder from the Buehler Co. in preparation for viewing in the polarizing optical microscope.

Surface Temperature

The surface temperature during fatiguing was measured with the Inframetrics Model 600 infrared thermal camera. The image consisted of a 2-dimensional map of temperature contours with a resolution of 0.02°C. The maximum temperature was at the region immediately ahead of the propagating crack. The temperature rise was obtained by taking the difference between the remote specimen temperature and the maximum temperature at the crack tip.

RESULTS AND DISCUSSION

Fatigue Crack Propagation (FCP)

The fatigue life time of the microlayer composites consists of a crack initiation period followed by a period of stable crack growth before fast, unstable crack propagation and fracture. The 49 and 776 layer composites have approximately the same fatigue life time, about 9000 cycles, although the number of cycles in the crack initiation and stable crack growth periods are different (Table I). For the initiation period, the 776 layer composite requires approximately 7100 cycles before the crack begins to grow whereas the 49 layer composite requires approximately 8300 cycles. On the other hand, the stable crack propagation period in the 776 layer composite is approximately 2.5 times longer than in the 49 layer composite, 1800 fatigue cycles vs. 700, and the stable crack grows further in the 776 layer composite, about 13.3 mm compared to about 9.7 mm. The results in Table I are averages of at least 15 fatigue experiments; in the following discussion data from single representative experiments are presented.

Figure 1 shows the increase in crack length as a function of the number of fatigue cycles after crack initiation. Plotted in this manner, the data show an initial slow growth region that persists for a larger number of cycles in the 776 layer composite. For example, it takes more than 1000 cycles after the crack has initiated for it to grow to 2 mm in length in the 776 layer composite compared to less than 500 cycles in the 49 layer composite. The better resistance of the 776 layer composite to fatigue crack growth can also be seen when the crack speed is plotted as a function of crack length (Fig. 2). The steady state plateau region above a crack length of about 2 mm is more pronounced in the 776 layer composite and persists to a crack length of almost 13 mm.

The resistance to FCP of the two composites can also be characterized by the fracture mechanics approach. In the following equations, J_1, K_1, and E

TABLE I
Fatigue Lifetime of Microlayer Composites

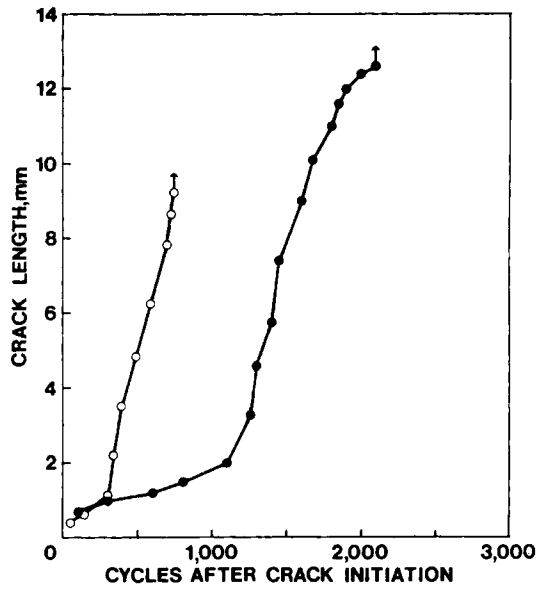|	49 Layer	776 Layer
Total cycles	9087 ± 472	8853 ± 388
Initiation	8302 ± 211	7158 ± 179
Propagation	707 ± 136	1867 ± 201
Stable crack length (mm)	9.7 ± 1.8	13.3 ± 1.2

Fig. 1. Fatigue lifetime of the 49 (O) and 776 (●) layer composites in fatigue cycles vs. crack length after crack initiation.

represent strain energy release rate, stress intensity factor, and tensile modulus, respectively, and L and B denote the crack length and specimen width. Then

$$J_1 = K_1^2/E \tag{1}$$

and

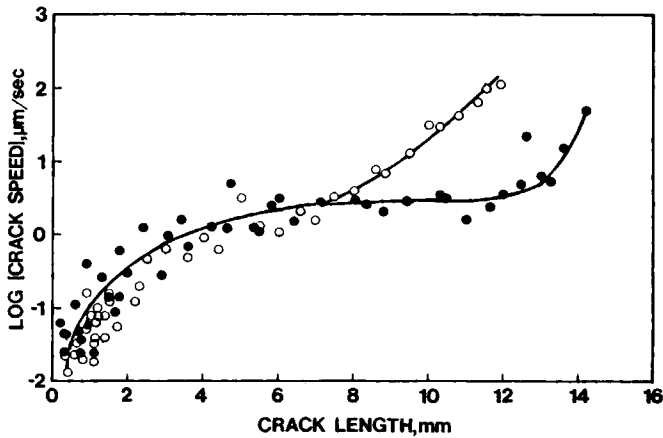$$K_1 = \sigma(\pi L)^{1/2} f(L/B) \tag{2}$$

Fig. 2. Crack speed of the 49 (O) and 776 (●) layer composites during stable crack propagation.

where the mean applied stress σ is 8.75 MPa and $f(L/B)$ is a geometric factor given by

$$f(L/B) = 1.12 - 0.231(L/B) + 10.55(L/B)^2$$
$$- 21.71(L/B)^3 + 30.39(L/B)^4 \quad (3)$$

for the specimen geometry used in this study.[12] The strain energy release rate is plotted against the crack growth per fatigue cycle in Figure 3. The critical strain energy release rate J_{1C} at the last cycle before catastrophic fracture is often regarded as a measure of the FCP resistance. This approach again demonstrates that the FCP resistance of the 776 layer composite, $J_{1C} = 34$ kJ/m^2, is higher than that of the 49 layer composite, $J_{1C} = 8$ kJ/m^2.

Damage Zone

The damage zone ahead of the propagating crack plays an important role in characterizing the FCP behavior of a material. Figure 4 shows the side view of the crack tip region of the 49 and 776 layer composites at a crack length of approximately 7 mm. These micrographs were taken when the fatigue cycle was at maximum load to identify the location of the crack tip. The crack tip is not always visible because of the jagged fracture surface, but can be located from the birefringent pattern. The damage zones are very different in appearance; ahead of the propagating crack in the 49 layer composite the zone is wider and longer than in the 776 layer composite. It appears that profuse crazing in the 49 layer composite is a dominant microdeformation process. In the 776 layer composite, a narrower, fork-shaped damage zone is observed with no crazing evident. In both cases, the damage zones are similar in appearance to those observed in SEN specimens during slow tensile loading.[4]

The microdeformation mechanisms in the damage zone can be seen more clearly in cross section. Figure 5(a) shows the damage zone of the 49 layer
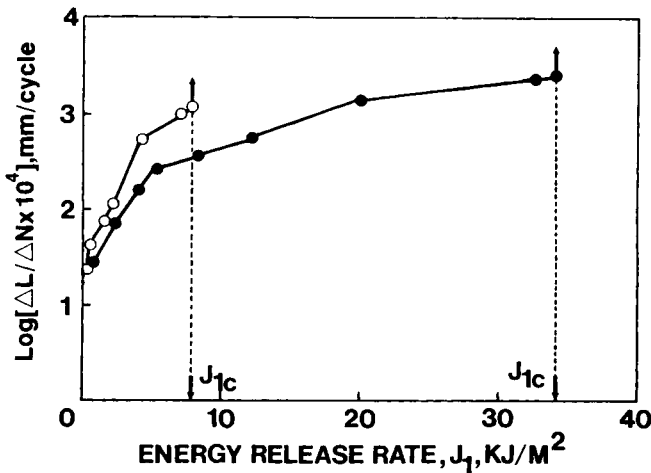

Fig. 3.   Strain energy release rate of the 49 (O) and 776 (●) layer composites vs. crack growth per fatigue cycle during stable crack propagation.
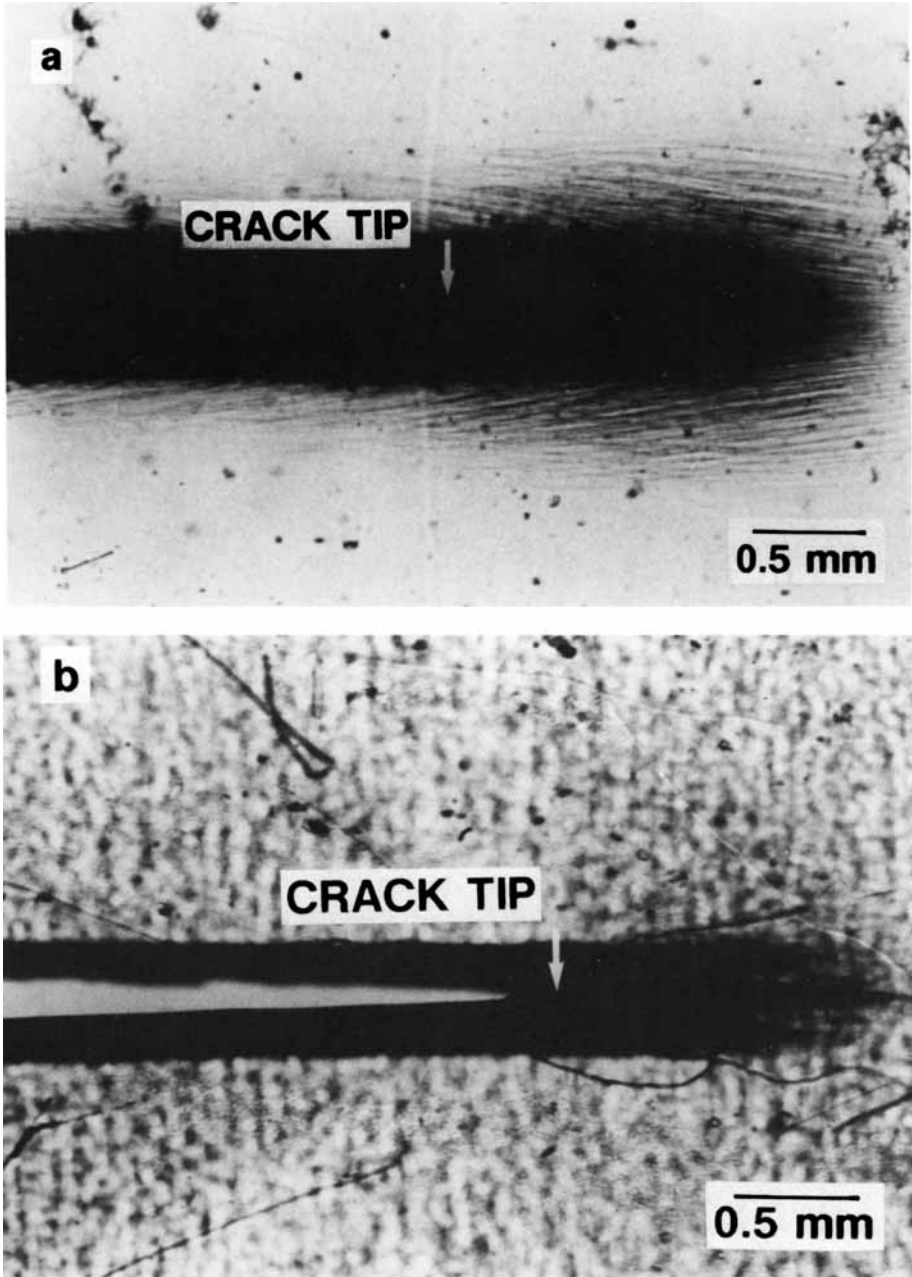
Fig. 4.   Side view of the damage zone ahead of the propagating crack in the (a) 49 and (b) 776 layer composites at maximum load and crack length of approximately 7 mm.

composite sectioned about midway between the crack tip and the tip of the damage zone when the crack length was approximately 2 mm. The highly damaged center line is the intersection with the parabolic crack plane. Extending above and below this line, crazing of the SAN layers constitutes the damage
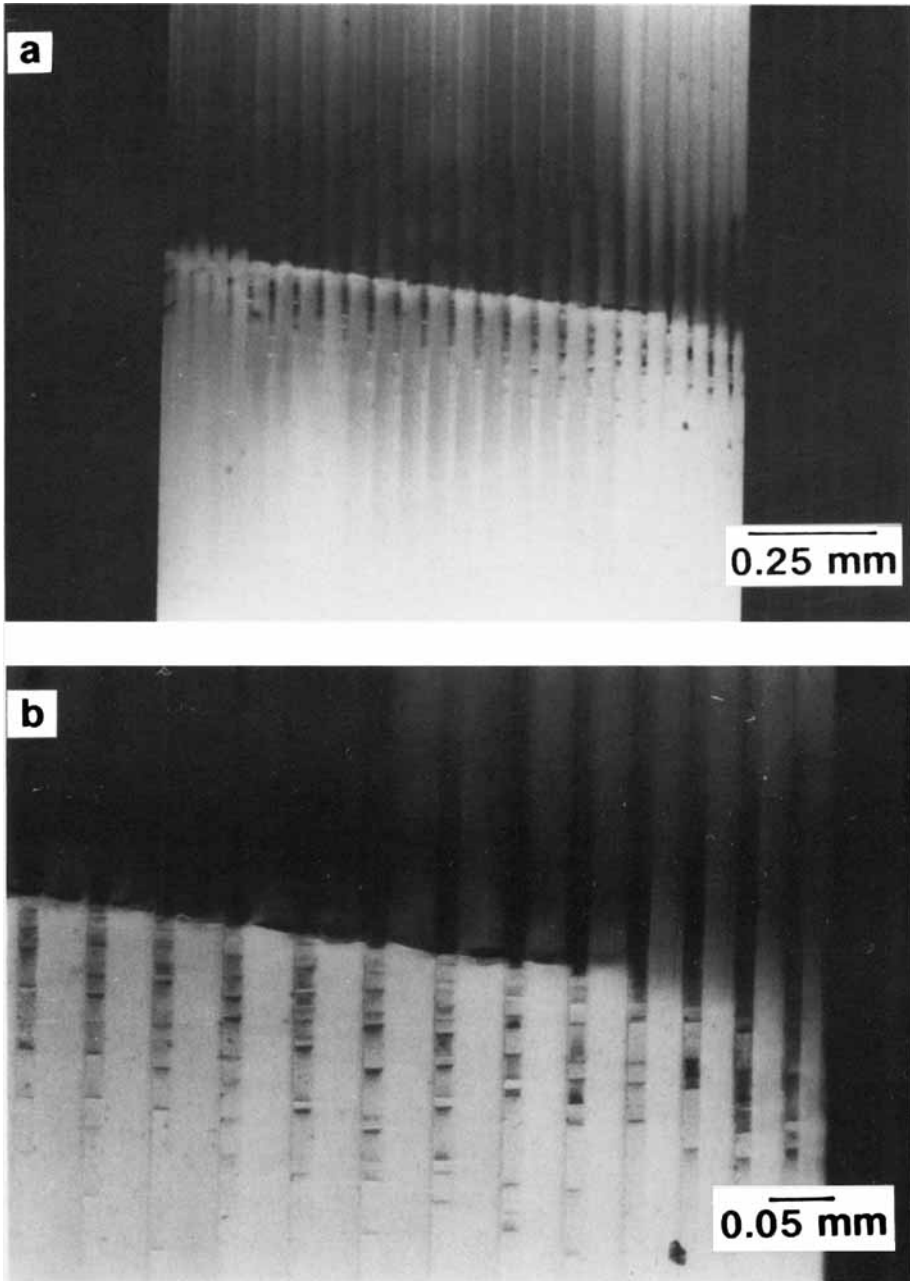
Fig. 5. Cross sectional view of the damage zone in the 49 layer composite. The section is midway between the crack tip and the end of the damage zone at crack length of approximately 2 mm: (a) lower magnification; (b) higher magnification.

zone. There is no visible deformation of the PC layers in the damage zone away from the crack line [Fig. 5(b)]. Because crazing of the SAN layers relieves constraints in the thickness direction, the damage zone extends uniformly through the thickness of the specimen and there is no reduction in thickness.

The cross section of the 776 layer composite is shown in Figure 6(a). Again, the section was made midway between the crack tip and the tip of the damage zone when the crack length was about 2 mm. The skin-core nature of the damage zone is evident. Two macroshear bands extend at about 50° from each
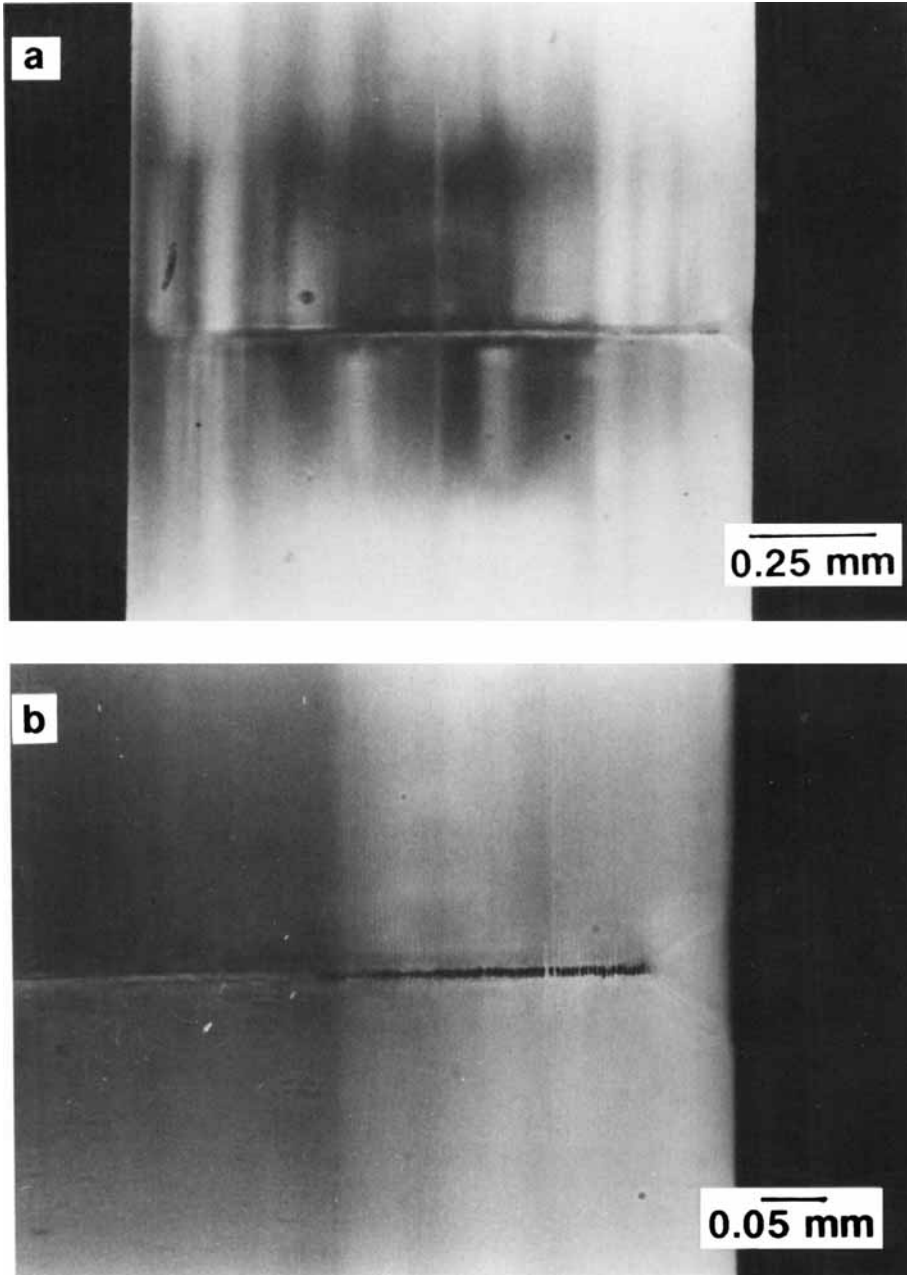

Fig. 6. Cross-sectional view of the damage zone in the 776 layer composite. The section is midway between the crack tip and the end of the damage zone at crack length of approximately 2 mm: (a) lower magnification; (b) higher magnification.

end of the highly damaged center crack line to the edge of the specimen. A higher magnification [Fig. 6(b)] shows that the shear bands extend through both PC and SAN layers. This manner of shear yielding of SAN layers under tensile loading is only observed when the layer thickness is small enough, on the order of microns, and has been shown to arise from a shear stress concentration at the interface produced by local shear yielding in the PC layer.[2]

Thinning of the specimen between the two shear bands confirms the plane stress condition in the skin region. The micrograph in Figure 6(b) also reveals the origin of the fork-shaped damage zone: the center "prong" arises from the center crack line while the two outer "prongs" are caused by light scattering from the surface contour where the shear bands intersect the edge of the specimen. The relative sizes of the plane stress skin region and the plane strain core region gradually change as the crack length increases. When the damage zone is viewed as in Figure 6(b), the origin of the shear bands moves inward toward the center as the crack length increases so that the distance between the shear bands when they intersect the surface becomes larger. When viewed from the side, this appears as an increase in the width of the damage zone. For example, the damage zone for the specimen in Figure 6(b) is smaller, about 0.1 mm, than that in Figure 4(b), about 0.5 mm.

The increase in damage zone width with crack length for both composites is shown in Figure 7. Note that the damage zone is larger in the 49 layer composite. Damage zone size does not correlate with FCP resistance in this case since the 49 layer composite has lower FCP resistance than the 776 layer composite. As indicated by the previous micrographs, the damage mechanisms are different in the two composites and it follows that more energy is absorbed per unit volume by the plastically deformed fork-shaped damage zone of the 776 layer composite than by the highly crazed zone of the 49 layer composite.

Fractography

Figure 8 shows a schematic representation of the fracture surfaces of the two composites. At the beginning of the crack growth, both composites show
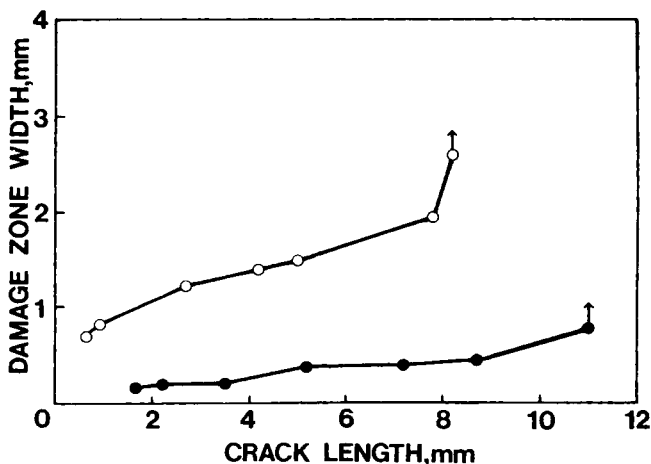

Fig. 7.   Damage zone width in the 49 (○) and 776 (●) layer composites vs. crack length during stable crack propagation.
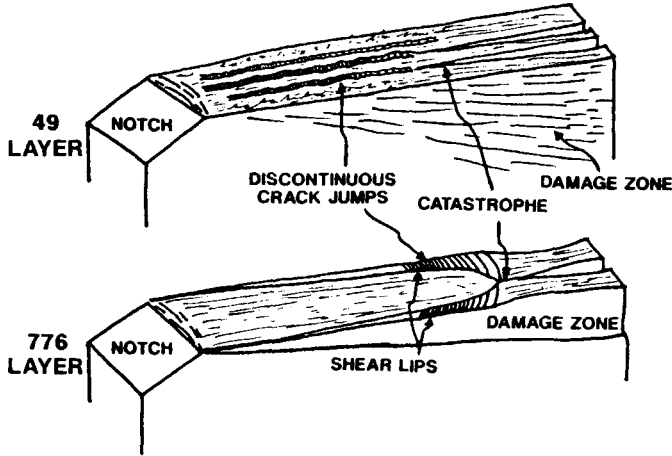
Fig. 8. Schematic representation of the fracture surface of the 49 and 776 layer composites. FCP direction is from left to right.

a flat fracture surface with several macroscopic crack jumps. This region correlates with the slow crack growth region observed at the beginning of FCP when the crack grows through the damage accumulated during the crack initiation period. The convex shape reveals the parabolic crack front that is characteristic of FCP. In the stable crack growth region, the fracture surface of the 49 layer composite shows a uniform texture across the thickness of the specimen whereas the 776 layer composite shows distinctive skin and core characteristics. There is no noticeable reduction in thickness of the 49 layer composite while considerable thinning within the region defined by the damage zone is observed with the 776 layer composite. At the point of catastrophic fracture, macroscopic delamination and splitting are observed in both composites. Several large splits are usually seen in the unstable crack propagation region of the 49 layer composite, while a single split forms in the center of the 776 layer composite.

Figure 9(a) shows an optical micrograph of the fracture surface of the 49 layer composite approximately midway along the region of stable crack propagation. Again the fracture surface shows the same overall features across the thickness. In some regions striations indicative of discontinuous crack jumps can be seen on drawn out PC layers. Details of the fracture surface are seen in a higher magnification SEM micrograph, Figure 9(b). The SAN layers show typical brittle fracture, whereas the PC layers are drawn out. The waviness of the PC layers, which corresponds to the striations in the previous optical micrograph, is not in registry from one PC layer to the next. These features of the fracture surface indicate that the layers of the 49 layer composite deform and fracture independently with no synergistic effects of the layered morphology. Extensive delamination is also apparent.

A cross section of the fracture surface taken in the stable crack growth region close to the point of catastrophic fracture (Fig. 10) illustrates the extent to which the PC layers are drawn and the amount of delamination. Features of this and preceding micrographs of the damage zone and subsequent fracture surface should correlate with the sequence of microdeformation events that occurs with increasing stress during tensile deformation of the 49 layer com-
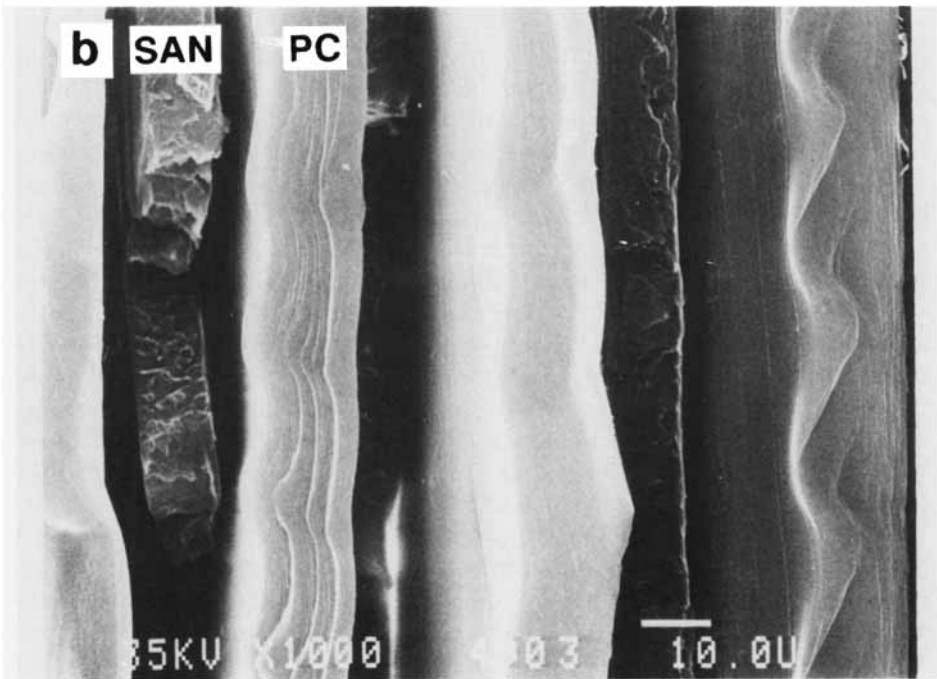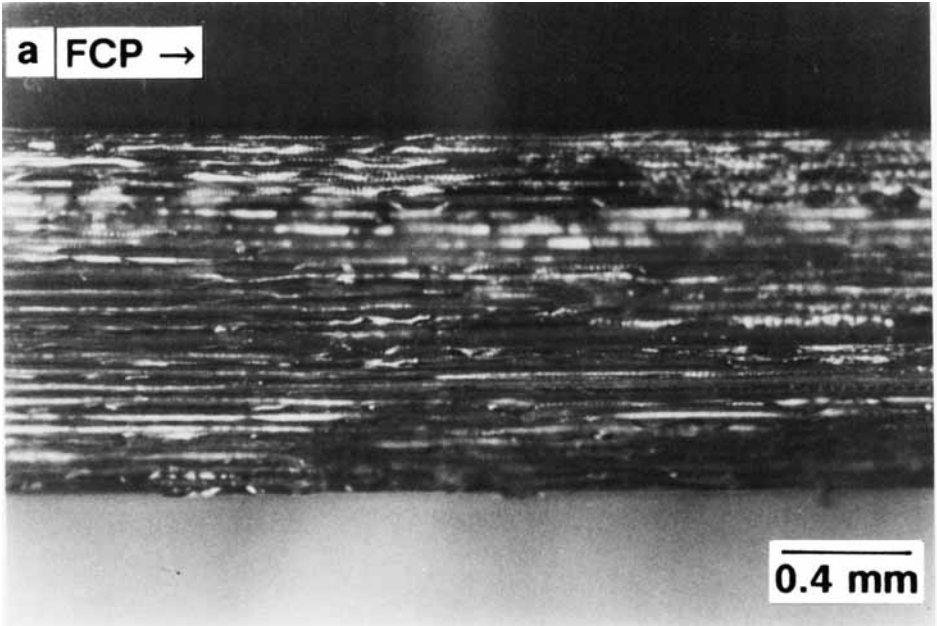
Fig. 9.   Fracture surface of the 49 layer composite midway along the region of the stable crack propagation: (a) overall view; (b) detail view.
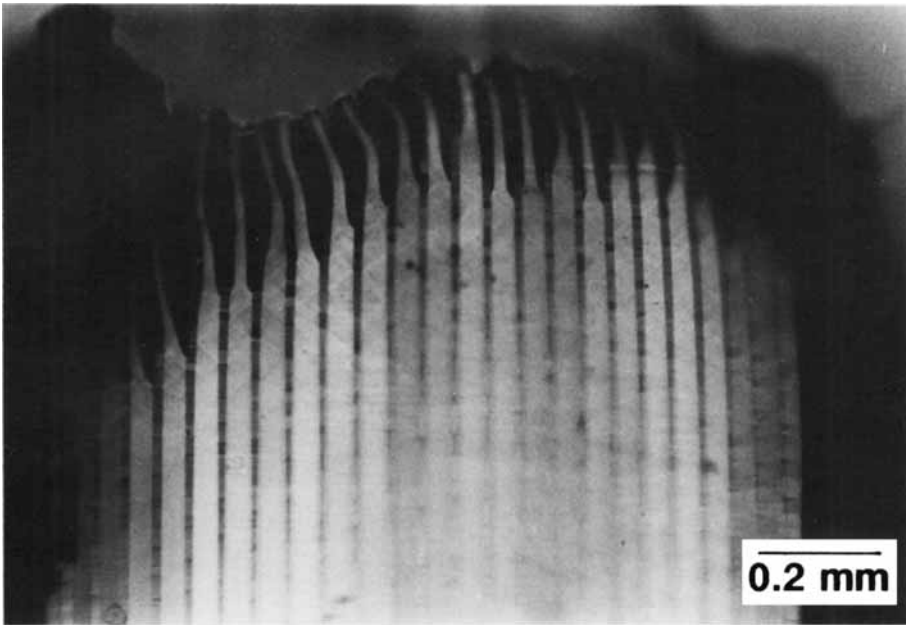
Fig. 10. Cross-sectional view of the fracture surface of the 49 layer composite. Section shown is near the point of catastrophic fracture.

posite. From previous studies, the first observable irreversible deformation event in the 49 layer composite is crazing or cracking of the SAN layers.[1,2] In the cross-sectional view of the damage zone (cf. Fig. 5), this occurs profusely along the crack growth line and also randomly away from the crack line to produce the damage zone. Because of good adhesion between PC and SAN layers, shear bands then initiate in the PC layers from the craze tips[1,2]; this is seen in the damage zone away from the fracture surface in Figure 10, which is more highly deformed than the damage zone in Figure 5. It is known from the previous studies that when the yield point is reached, cold drawing of the PC layers occurs while the SAN layers fracture in a brittle manner. In the fatigue experiment, this means that during crack propagation, PC layers are drawn across the crack opening and remain load bearing after the SAN layers have fractured. This serves to delocalize stress at the crack tip.[1] The highly drawn PC layers observed on the fracture surface in Figure 10 indicate that this mechanism contributes to FCP resistance of the 49 layer composite.

The fracture surface of the 776 layer composite from the region of stable crack propagation is shown in Figure 11(a). The shear lips are clearly evident with the stop-start crack growth striations that extend smoothly across the many layers that comprise the shear lip. The width of the shear lips and the distance between striations increase as the crack grows. The shear lips are featureless when the fracture surface is viewed at higher magnification in the SEM [Fig. 11(b)], while extensive delamination occurs in the core region. A higher magnification of the core region, [Fig. 11(c)] shows that the SAN layers do not fracture in a brittle manner, as in the 49 layer composite, but are highly drawn as are the PC layers.
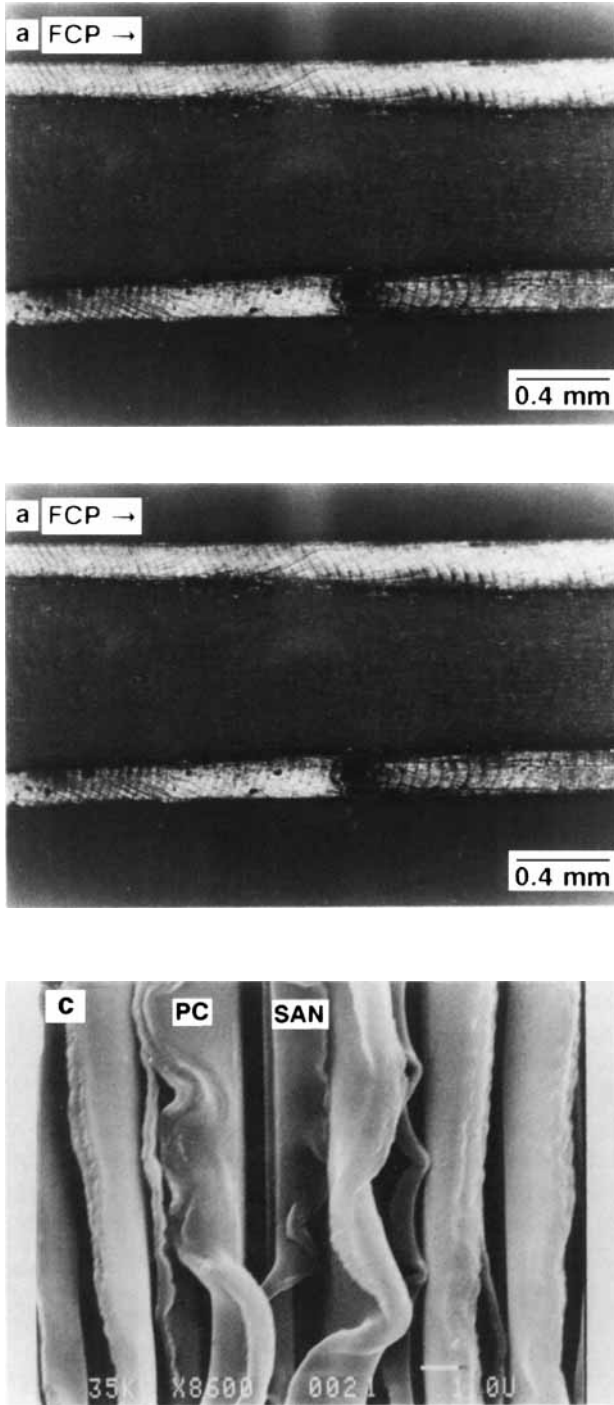
Fig. 11.   Fracture surface of the 776 layer composite midway along the region of the stable crack propagation: (a) overall view; (b, c) detail views.

A cross section of the fracture surface of the 776 layer composite from the stable crack growth region close to the point of catastrophic fracture is shown in Figure 12. Two large cracks observed between the shear lips and the center region of the fractured specimen relieve constraints in the thickness direction and during fracture the material in the shear lips is highly drawn without delamination. The material in the center region is also drawn but not to the same extent as the shear lips. Thickness constraints in this region produce extensive delamination. These characteristic features of the fracture surface are derived from the skin–core nature of the damage zone [cf. Fig. 6(a)]. In particular, the prominant shear lips originate from the macroshear bands of the skin region, while the less highly drawn center region is derived from the center crack line.

Crack Tip Temperature

Maximum surface temperature in the region immediately ahead of the propagating crack is plotted in Figure 13. An increase in temperature is detected during only the final four cycles of stable crack propagation in the 49 layer composite, whereas there is a measurable temperature increase during the final 172 cycles in the fatigue life time of the 776 layer composite. This temperature increase occurs during the final 4 mm of stable crack growth which approximately corresponds to the additional length of stable crack growth for the 776 layer composite. The temperature increase is generally in the range of 1–5°C except for the last cycle during which fracture occurs and the temperature rise may be 20°C or more.
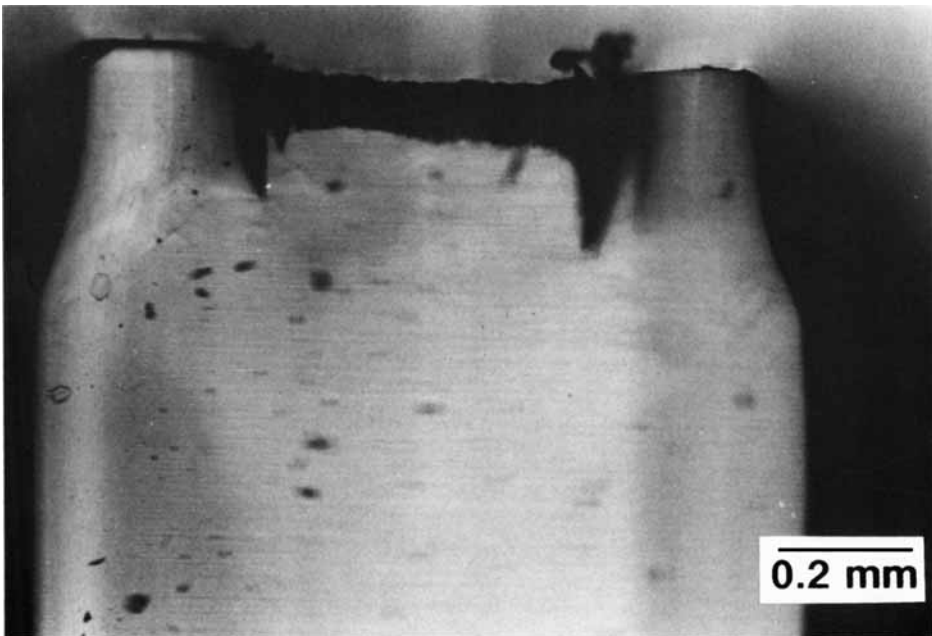

Fig. 12.   Cross-sectional view of the fracture surface of the 776 layer composite. Section shown is near the point of catastrophic fracture.
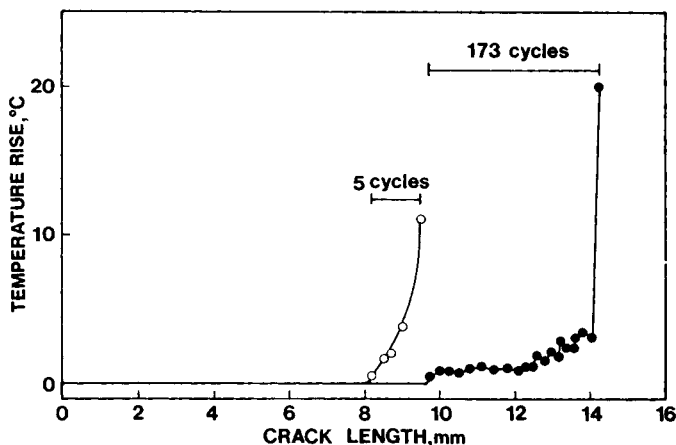
Fig. 13.   Maximum surface temperature ahead of the propagating crack in the 49 (○) and 776 (●) layer composites vs. crack length.

The temperature at the crack tip is shown cycle by cycle in Figure 14 for the 776 layer composite during the final 172 cycles of stable crack propagation. The temperature oscillates with an average of four cycles per oscillation. The temperature fluctuation increases gradually from about 0.5 to 1.5°C close to fracture, but the four cycle period remains constant. The distance the crack would propagate during a single temperature oscillation, calculated from the measured macroscopic crack speed, correlates with the spacing of striations on the shear lips. It follows that the temperature oscillations represent stepwise microfracture in the shear lips, where damage accumulates for three cycles and the crack jumps on the fourth cycle with the peak temperature. Dissipation of mechanical energy as heat by plastic deformation and ductile fracture mechanisms in the shear lips would seem to be responsible for the greater FCP
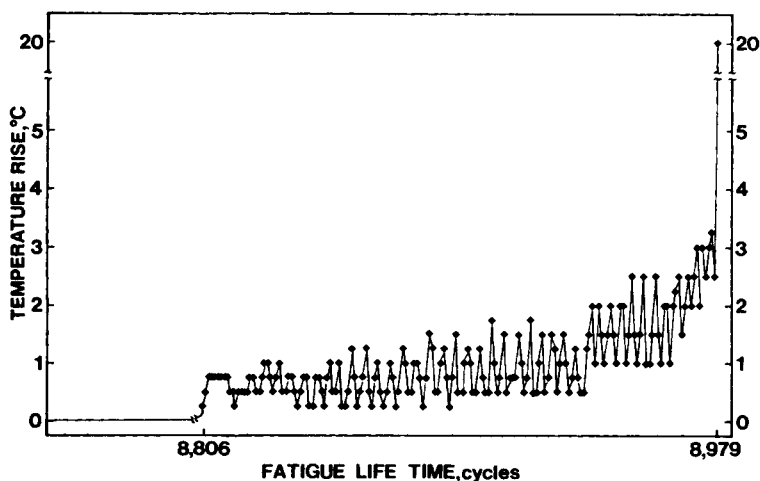

Fig. 14.   Surface temperature ahead of the propagating crack in the 776 layer composite during the last 172 cycles. Each square represents a single cycle.

resistance of the 776 layer composite as reflected by the higher value of J_{1C}. The effect is most noticeable at higher crack lengths beginning at approximately the crack length where the 49 layer composite fractures catastrophically; experimentally the effect produces a plateau in crack speed and an additional 3–4 mm of stable crack growth.

CONCLUSIONS

This study of the effect of layer thickness on the fatigue crack propagation resistance of PC/SAN microlayer composites leads to the following conclusions:

1. When the composition and sheet thickness are the same, the composite with 776 layers possesses better resistance to FCP than the 49 layer composite.

2. The SAN and PC layers in the 49 layer composite deform and fracture independently by crazing and shear banding, respectively. Resistance to FCP is provided by drawing out of the PC layers across the growing crack.

3. Synergistic effects of the layered morphology result in shear deformation of both SAN and PC layers in the 776 layer composite. Better FCP resistance is due to extensive plastic deformation in the damage zone ahead of the crack and ductile fracture with formation of shear lips.

References

1. B. Gregory, J. Im, A. Hiltner, and E. Baer, *J. Mater. Sci.*, **22**, 532 (1987).

2. M. Ma, J. Im, A. Hiltner, and E. Baer, *J. Mater. Sci.*, **25**, (1990), to appear.

3. J. Im and A. Hiltner, in *High performance Polymers*, E. Baer and A. Moet, Eds., Hanser International, Munich, 1990.

4. M. Ma, Ph.D thesis, Case Western Reserve University, Cleveland, OH, 1988.

5. R. W. Hertzberg and J. A. Manson, *Fatigue of Engineering Plastics*, Academic, New York, 1980.

6. C. B. Bucknall and W. W. Stevens, *J. Mater. Sci.*, **15**, 2950 (1980).

7. J. A. Sauer and G. C. Richardson, *Int. J. Fract.*, **6**, 499 (1980).

8. A. Chudnovsky, A. Moet, R. J. Bunkert, and M. T. Takemori, *J. Appl. Phys.*, **54**, 5562 (1983).

9. M. T. Takemori, *Ann. Rev. Mater. Sci.*, **14**, 171 (1984).

10. J. F. Mandell and J. P. F. Chevaillier, *Polym. Eng. Sci.*, **25**, 170 (1985).

11. J. C. Radon, *Int. J. Fact.*, **16**, 533 (1980).

12. H. Tada, P. C. Paris, and G. P. Irwin, in *The Stress Analysis of Cracks Handbook*, Del Research Corp., Helertown, PA, 1973.